Progress in Earth and Planetary Science

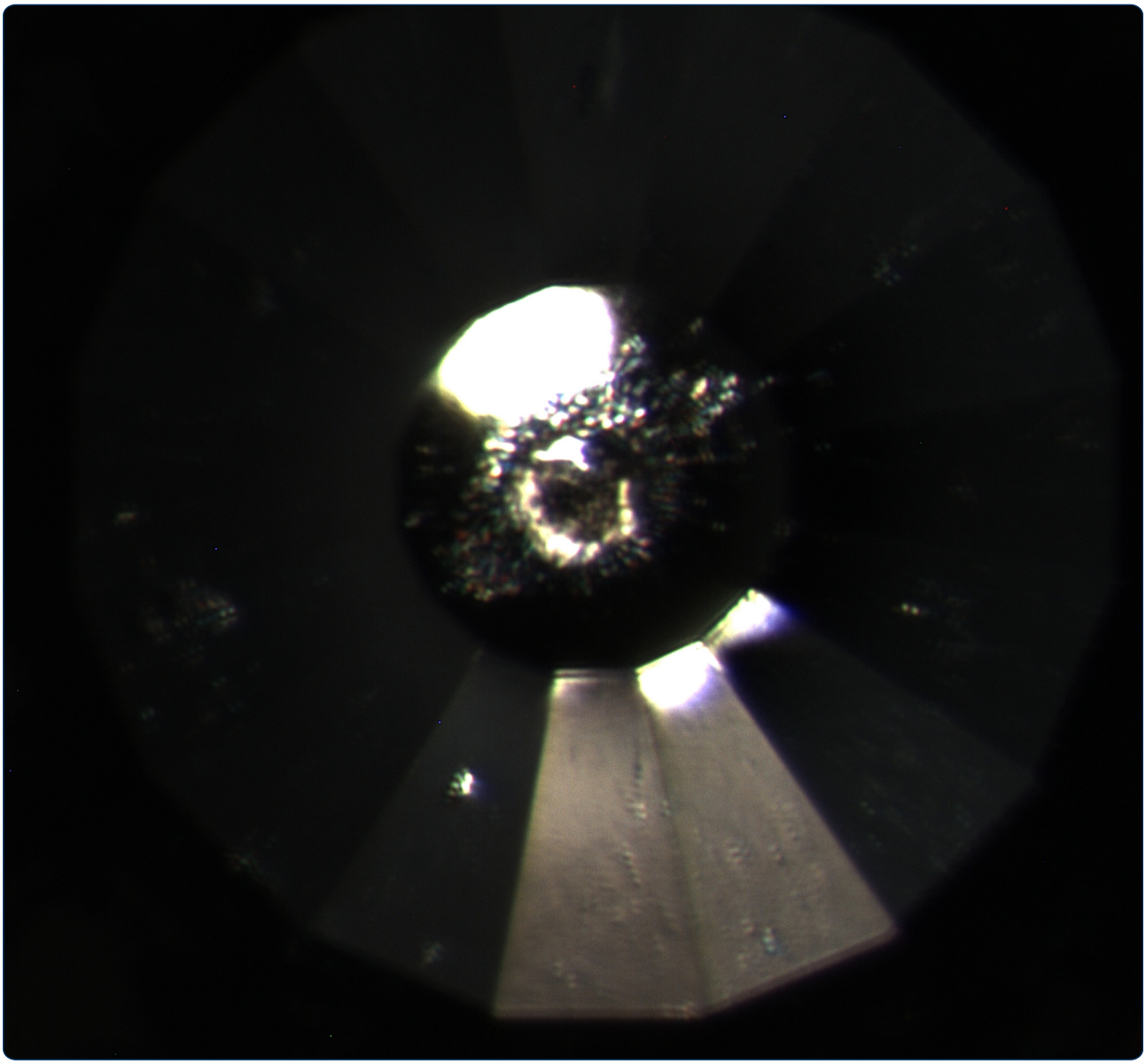

Unit cell determination of coexisting post-perovskite and H-phase in $(Mg,Fe)SiO_3$ using multigrain XRD: compositional variation across a laser heating spot at 119 GPa

Zhang *et al.*

Springer Open

Zhang *et al. Progress in Earth and Planetary Science* (2016) 3:13

DOI 10.1186/s40645-016-0091-8

Zhang et al. Progress in Earth and Planetary Science (2016) 3:13
DOI 10.1186/s40645-016-0091-8

Progress in Earth and Planetary Science

RESEARCH ARTICLE Open Access

Unit cell determination of coexisting post-perovskite and H-phase in $(Mg,Fe)SiO_3$ using multigrain XRD: compositional variation across a laser heating spot at 119 GPa

Li Zhang[1*], Yue Meng[2] and Ho-kwang Mao[1,3]

Abstract

Multigrain X-ray diffraction (XRD) can be used to accurately calculate the unit cell parameters of individual mineral phases in a mineral assemblage contained in a diamond anvil cell (DAC). Coexisting post-perovskite (ppv) and H-phase were synthesized at 119 GPa and 2500 K from $(Mg_{0.85}Fe_{0.15})SiO_3$ in a laser-heated DAC. The unit cell parameters of the ppv and coexisting H-phase were determined using multigrain XRD with a 5 μm spatial resolution, close to the size of the X-ray beam, to understand compositional variations across the center area (20–30 μm) in a laser-heated sample. The ppv phase was Fe-depleted and the unit cell volume of ppv decreased by only 0.16 % (corresponding to ~3 % variation of $FeSiO_3$) from the heating center to 10 μm off the center, while the sample pressure remained at 119 GPa in a Ne quasi-hydrostatic environment. The unit cell volume of the H-phase decreased by 0.54 % (~10 % variation of FeSiO3 content) over the same 10 μm distance. Both phases were more Fe-enriched in the slightly hotter center. This observation suggests that thermal diffusion may not be the major driver for the compositional variations of ppv and H-phase in the center portion of a laser-heated sample. Instead, these variations could be caused by a temperature effect on the partitioning between the ppv and H-phase over the small gradient.

Keywords: Lower mantle, Multigrain XRD, Diamond anvil cell, Post-perovskite, H-phase, Unit cell, Synchrotron X-ray

Background

High-pressure (P) and high-temperature (T) experiments conducted in a laser-heated diamond anvil cell (DAC) have been widely used to simulate the extreme conditions in the Earth's interior. Integrating a laser-heated DAC with synchrotron X-ray diffraction (XRD) remains the dominant tool for studies of high-P mineral physics. In situ unit cell determination of minerals under high P-T conditions is a common task in the laser-heated DAC experiments. In an experiment involving element partitioning and/or chemical reaction, unit cell parameters often reflect compositional changes due to differences in the atomic radii of the elements involved. In the past decade, the combination of focused ion beam (FIB) with transmission electron microscopy (TEM) or other analytical techniques (Miyahara et al. 2008; Sinmyo et al. 2008) has been used to analyze the chemical compositions of samples recovered from a laser-heated DAC. This approach could allow the phase identification and detailed chemical analysis of materials under high P-T conditions, provided that all the phases and their chemical compositions remain unchanged after T quench from heating and during decompression to ambient conditions and that they remain unaffected by the FIB/TEM processes. On the other hand, in situ characterization is essential for obtaining information regarding phase changes and unit cell variations induced by pressure and composition.

In situ determination of unit cell parameters and crystal chemistry remains a challenge as pressure exceeds 100 GPa and temperature reaches several thousand kelvins (K).

* Correspondence: zhangli@hpstar.ac.cn
[1]Center for High Pressure Science and Technology Advanced Research (HPSTAR), Shanghai 201203, China
Full list of author information is available at the end of the article

Small sample sizes together with the re-crystallization of coexisting phases to coarse grains after laser heating significantly degrade the powder diffraction patterns required for accurate data analysis. In recent years, the multigrain method (Sørensen et al. 2012) has been successfully applied to study coarse-grained polycrystalline samples obtained under ultra-high *P-T* conditions in a DAC (Nisr et al. 2012; Zhang et al. 2013; Zhang et al. 2014; Rosa et al. 2015; Zhang et al. 2016). These studies have demonstrated that integration of the multigrain method with synchrotron XRD is suitable for treating each sub-micron-sized crystallite as a single crystal in a coarse-grained polycrystalline material in a DAC. In this study, we provide a detailed analysis of the unit cell parameters of Fe-depleted bridgmanite from multiple grains. Furthermore, the unit cell parameters of the coexisting post-perovskite (ppv) and H-phase, quenched from laser heating at 119 GPa, were calculated using multigrain XRD to determine the spatial variation of the compositions of individual phases across a laser heating spot.

Methods

An orthopyroxene (opx) sample with a composition of $(Mg_{0.85}Fe_{0.15})SiO_3$ (Fs15) was used as the starting material in the two experiments reported in this study. Diamond anvils with flat culet diameters of 150 μm beveled at 10° up to 300 μm were mounted in Boehler seats with up to a 60° opening. A piece of opx sample was pre-compressed into a disk of ~10 μm thickness, cut to 40–60 μm in diameter, and placed in a ~60 μm diameter Re gasket hole in a Mao-type symmetric DAC for each experiment. Compressed Ne was loaded as the pressure transmitting media for use as a pressure scale (Fei et al. 2007) and thermal insulation layer during laser heating. XRD measurements were conducted at the high-pressure synchrotron 16ID-B and 13ID-D beamlines of the advanced photon source (APS), Argonne National Laboratory.

To achieve the best possible uniform heating and data quality, and to minimize the temperature gradient in a relatively large sample area, samples were prepared with careful attention to details. Firstly, the heating spot size was adjusted to cover most of the sample in a DAC (Meng et al. 2015) and a heating spot with an almost flat area of ~30 μm was used for sample synthesis at the 16-ID-B beamline. Secondly, to achieve good coupling of the sample with the laser beam, efforts were made to control uniformity of the sample thickness, chemical homogeneity of the starting material, and the symmetric insulation layers of the quasi-hydrostatic Ne medium. The opx sample was prepared by compressing a single crystal, and thus, sample homogeneity and non-porosity was ensured. The sample was then successfully sandwiched between symmetric insulation layers of Ne from both sides. Note that the use of a quasi-hydrostatic medium such as Ne can speed up phase equilibrium. Spotty diffraction patterns were obtained, which indicated grain growth, after heating for only 2 min, in contrast to the 30–60 min required for experiments above 100 GPa reported in a previous study (Sinmyo et al. 2008). In situ XRD measurements indicated no obvious changes in the sample between heating for 2 and 10 min; therefore, a short duration of heating was used to avoid chemical segregation.

After successful sample synthesis, we aligned the sample to the ω-rotation center and collected a set of two-dimensional multigrain XRD patterns at small increments of the rotation angle over the maximum X-ray accessible range, similar to the rotation method used in conventional single-crystal crystallography. The FABLE package (Sørensen et al. 2012) was used to process the spotty XRD patterns, and the orientation matrices of individual grains were indexed using the GrainSpotter algorithm (Schmidt 2014).

Results and discussion

Unit cell determination of $(Mg,Fe)SiO_3$ bridgmanite coexisting with H-phase

Fe depletion in bridgmanite was observed as a result of the disproportionation of Fe-bearing bridgmanite and the appearance of an Fe-rich H-phase in a quasi-hydrostatic Ne medium (Zhang et al. 2014). XRD patterns were collected with an X-ray wavelength of 0.3738 Å by rotating the DAC from −21° to 21° in 0.1° steps at the 16ID-B beamline. The exposure time was 20 s/frame. A total of 51 grains of bridgmanite were indexed and the 16 of them with the most reflections available were selected for unit cell determination (Table 1). The 16 grains were then divided into three groups. A total of 150–180 reflections were merged from the five or six grains in each group and the unit cell parameters were refined from these reflections using UNITCELL (Holland and Redfern 1997), as shown in Table 1. The 5 grains in group #1 were orientated with reasonable constraints on all *a*, *b*, and *c* lattice parameters for individual grains, and the standard deviation was 0.23 $Å^3$ for the 5 unit cell volumes of each grain. In contrast, another 5 grains in groups #2 and 6 grains in group #3 showed weak constraints on certain directions of the lattice due to their orientations relative to the DAC opening. The unit cell volumes calculated from individual grains in group #2 and group #3 showed scattered values with standard deviations of 0.37 $Å^3$ for the 5 grains in group #2 and 0.89 $Å^3$ for the 6 grains in group #3. These results indicate that weak constraints on certain directions of the lattice of an individual grain could cause a large deviation in its unit cell volume, suggesting that unit cell determination from one crystal in conventional single-crystal XRD may suffer from a similar problem. Multigrain XRD overcomes this problem by merging enough reflections from several grains that have random orientations to determine the unit cell

Table 1 Unit cell parameters for Fe-depleted bridgmanite coexisting with H-phase at 102.5 GPa

Grain no.	*N*	*a* (Å)	σ (*a*)	*b* (Å)	σ (*b*)	*c* (Å)	σ (*c*)	*V* (Å^3)	σ (*V*)
Group #1									
12	39	4.6049	0.0006	6.3381	0.0018	4.3580	0.0008	127.19	0.03
17	30	4.6014	0.0019	6.3536	0.0010	4.3521	0.0010	127.24	0.04
32	38	4.6096	0.0009	6.3275	0.0012	4.3822	0.0011	127.82	0.03
35	38	4.6088	0.0014	6.3321	0.0013	4.3727	0.0006	127.61	0.02
43	36	4.6104	0.0008	6.3482	0.0011	4.3552	0.0011	127.47	0.03
Merged	181	4.6074	0.0004	6.3398	0.0005	4.3658	0.0004	127.52	0.01
Group #2									
6	38	4.6021	0.0018	6.3459	0.0018	4.3713	0.0004	127.66	0.03
16	51	4.6413	0.0020	6.3345	0.0011	4.3629	0.0003	128.27	0.04
23	33	4.5927	0.0015	6.3876	0.0039	4.3607	0.0004	127.93	0.05
24	33	4.5966	0.0024	6.3271	0.0024	4.3732	0.0004	127.19	0.03
29	31	4.6130	0.0029	6.3361	0.0019	4.3619	0.0006	127.49	0.05
Merged	185	4.6063	0.0007	6.3391	0.0007	4.3655	0.0002	127.47	0.01
Group #3									
33	28	4.6627	0.0066	6.3463	0.0008	4.3566	0.0005	128.92	0.17
36	30	4.5777	0.0027	6.3570	0.0017	4.3688	0.0005	127.13	0.05
41	33	4.5978	0.0011	6.4384	0.0061	4.3615	0.0004	129.11	0.10
46	27	4.5738	0.0027	6.3686	0.0024	4.3609	0.0005	127.03	0.05
51	18	4.6037	0.0010	6.3269	0.0017	4.3640	0.0018	127.11	0.04
1	23	4.5907	0.0024	6.3631	0.0013	4.3562	0.0011	127.25	0.04
Merged	158	4.6025	0.0005	6.3501	0.0005	4.3625	0.0002	127.50	0.01

N is the number of reflections. Sixteen grains were divided into three groups

parameters of each phase (Zhang et al. 2016). The refined unit cell parameters from merged reflections in each group did lead to consistent results, with a unit cell volume of 127.52(1) Å^3 in group #1, 127.47(1) Å^3 in group #2, and 127.50(1) Å^3 in group #3. The analysis demonstrated that the unit cell parameters of a high-*P* phase can be well constrained from enough merged reflections of several grains that have different orientations in a quasi-hydrostatic sample environment.

The unit cell parameter of Ne after *T* quench from 2300 K was calculated from three diffraction lines, 111, 200, and 220, and $a = 2.962$ (7) Å. The corresponding pressure was 102.5 GPa using the Vinet pressure scale of Ne (Fei et al. 2007). The Fe content in bridgmanite after disproportionation was characterized as $x = 0.02(2)$ in $(Mg_{1-x},Fe_x)SiO_3$ bridgmanite by ex situ FIB-TEM (Zhang et al. 2014). The unit cell volume of the Fe-depleted bridgmanite lies on the *P-V* curve of Fe-free $MgSiO_3$ bridgmanite (Lundin et al. 2008), as shown in Fig. 1, indicating consistency between the Vinet pressure scale of Ne (Fei et al. 2007) and the Au scale (Tsuchiya 2003). On the other hand, a previous study (Lundin et al. 2008) confirmed the consistency between the Au scale (Tsuchiya 2003) and another Au scale (Dewaele et al. 2004); the latter Au scale (Dewaele et al. 2004) agrees well with the internally consistent Au and Ne scales by Fei et al. (2007). However, the unit cell volume of $(Mg_{0.91}Fe_{0.09})SiO_3$ bridgmanite at 100 GPa (Dorfman et al. 2013) using the Au scale (Fei et al. 2007) is even slightly lower than that of Fe-free bridgmanite (Lundin et al. 2008) (Fig. 1), although the pressure scales used in

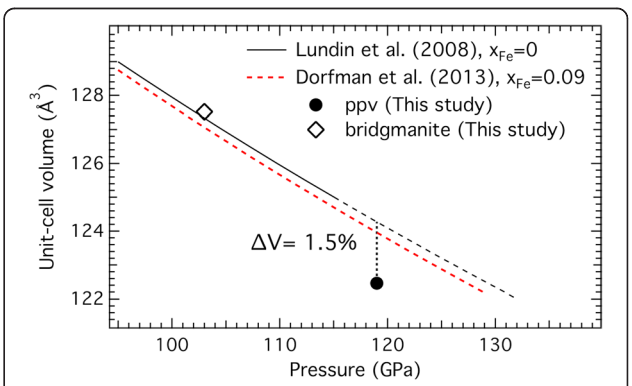

Fig. 1 Unit cell volumes of $(Mg,Fe)SiO_3$ bridgmanite and ppv versus pressure. The unit cell volumes of the Fe-depleted bridgmanite at 102.5 GPa and the ppv phase at 119 GPa coexisting with the H-phase are compared with the equations of state for Fe-free $MgSiO_3$ bridgmanite (Lundin et al. 2008) and $(Mg_{0.91}Fe_{0.09})SiO_3$ bridgmanite (Dorfman et al. 2013)

these two studies are consistent. The reason for this discrepancy is unclear. Multigrain XRD may have significant advantages over powder XRD for determining equations of state if one consistent pressure scale is used at all pressures and a quasi-hydrostatic sample environment is maintained.

Unit cell variations of coexisting ppv and H-phase across a laser heating spot

The coexisting ppv and H-phase were synthesized from $(Mg_{0.85}Fe_{0.15})SiO_3$ at 119 GPa (P after T quench) and 2500 K. After T quench and at 119 GPa, multigrain XRD data were collected for each sample position from the heating center to the margin, at steps of 5 μm across a laser heating spot. Diffraction patterns in step scans at each sample position were collected at ω increments of 0.25° over the DAC opening of 50°. The micro-focused XRD beam available at the 13ID-D beamline had a spot size of 3 by 4 μm with an X-ray wavelength of 0.3344 Å, and the exposure time was only 2 s/frame. The unit cell parameters of $(Mg,Fe)SiO_3$ ppv at each sample position were determined from ~150 reflections merged from several grains, as shown in Table 2 and Fig. 2a. The unit cell volume of ppv decreased by only 0.16 % from the heating center to 10 μm off the center, and the sample pressure remained at 119 GPa in the Ne quasi-hydrostatic environment. According to the previously determined relationship between the $FeSiO_3$ content in ppv and the equations of state (Zhang et al. 2012), the 0.16 % change in the unit cell volume of ppv corresponds to a ~3 % change of $FeSiO_3$ at 119 GPa, regardless of the absolute pressure determined by the different pressure scales. The unit cell volume of ppv in the heating center is also plotted in Fig. 1 and compared with the equation of state for Fe-free bridgmanite (Lundin et al. 2008). The unit cell volume of ppv is 1.5 % smaller than the value calculated from the equation of state for Fe-free bridgmanite and is consistent with the volume change from the bridgmanite to ppv transition in Fe-free $MgSiO_3$ (Tsuchiya et al. 2004). Fe depletion in ppv is confirmed when coexisting with H-phase.

H-phase was observed coexisting with ppv from the heating center to 10 μm off the center. The peak intensities of H-phase were comparable with those of the ppv phase. The unit cell volume of H-phase decreased by 0.54 % from the center to 10 μm off the center, as shown in Table 3 and Fig. 2b, suggesting a larger compositional variation in H-phase over the same distance. The relationship between the $FeSiO_3$ content and the equations of state for H-phase has not yet been established. Assuming that the effect of the $FeSiO_3$ content on the unit cell volume of H-phase is comparable to that of bridgmanite or ppv, the variation of $FeSiO_3$ content in H-phase is estimated as 9–14 %, based on the relationship between the $FeSiO_3$ content in ppv and their equations of state (Zhang et al. 2012) or 8–10 % based on the similar relationship to bridgmanite (Dorfman et al. 2013), corresponding to the 0.54 % change of the unit cell volume of H-phase.

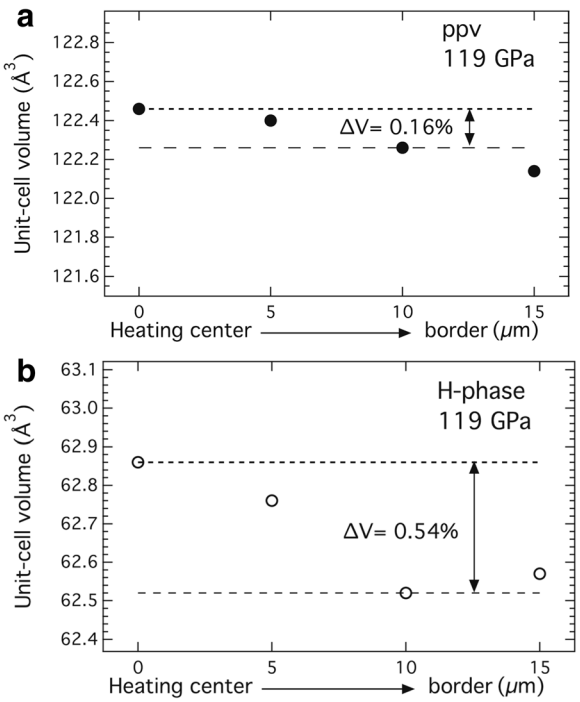

Fig. 2 Unit cell volumes of coexisting $(Mg,Fe)SiO_3$ ppv and H-phase across a laser heating spot. The unit cell volumes of **a** $(Mg,Fe)SiO_3$ ppv and **b** H-phase obtained using multigrain XRD are plotted as function of distance from the heating center to the margin at steps of 5 μm in a laser-heated sample at 119 GPa. The unit cell volumes of ppv and H-phase decrease by 0.16 and 0.54 %, respectively, from the center to 10 μm off the center, while the sample pressure remained the same in the Ne quasi-hydrostatic environment

Table 2 Variations of unit cell parameters for $(Mg,Fe)SiO_3$ ppv across a laser-heated spot at 119 GPa. The unit cell volume of the ppv phase slightly decreased by 0.16 % over the 10 μm distance from the center to the margin in the heated spot. N is the number of reflections from multiple grains at each sample position

Sample position	N	a (Å)	σ (a)	b (Å)	σ (b)	c (Å)	σ (c)	V (Å^3)	σ (V)	aNe (Å)	σ (a)	P (GPa)
Heating center	136	2.4654	0.0002	8.1156	0.0005	6.1207	0.0004	122.46	0.01	2.923	0.005	119
5 μm off center	170	2.4647	0.0001	8.1180	0.0004	6.1173	0.0005	122.40	0.01	2.924	0.004	119
10 μm off center	155	2.4644	0.0001	8.1078	0.0008	6.1190	0.0004	122.26	0.01	2.924	0.006	119
15 μm off center	176	2.4644	0.0002	8.0986	0.0005	6.1200	0.0004	122.14	0.01	2.920	0.011	120

Table 3 Variations of unit cell parameters for H-phase across a laser-heated spot at 119 GPa. The unit cell volume of the H-phase coexisting with the ppv gradually decreased by 0.54 % over the same 10 μm distance from the center to the margin in the heated spot. *N* is the number of reflections from multiple grains at each sample position

Sample position	*N*	*a* (Å)	σ (*a*)	*c* (Å)	σ (*c*)	*V* (Å^3)	σ (*V*)	*a*Ne (Å)	σ (*a*)	*P* (GPa)
Heating center	71	5.0674	0.0003	2.8265	0.0003	62.86	0.01	2.923	0.005	119
5 μm off center	101	5.0665	0.0002	2.8232	0.0003	62.76	0.01	2.924	0.004	119
10 μm off center	71	5.0577	0.0004	2.8220	0.0003	62.52	0.01	2.924	0.006	119
15 μm off center	120	5.0624	0.0002	2.8192	0.0003	62.57	0.01	2.920	0.011	120

Previous studies using ex situ TEM analysis of recovered samples found that the compositions of ppv were approximately constant for the entire hot spot, while ferropericlase exhibited significantly larger spatial variations in iron content with FeO migration to the cold region (Sinmyo et al. 2008), indicating that the effect of thermal diffusion on an individual phase is related to its Mg-Fe interdiffusion rate. However, both ppv and H-phase in the present sample are more Fe-enriched in the slightly hotter center. The ppv phase is Fe-depleted with ~3 % variation of $FeSiO_3$ over the 10 μm distance, whereas the compositional variation in the coexisting H-phase is nearly three times of that in the ppv over the same distance. This observation suggests that thermal diffusion may not be the major driver for the compositional variations of ppv and H-phase in the center portion of the laser-heated sample. Instead, temperature effects on the partitioning behavior over a small gradient could explain the partitioning behavior between ppv and H-phase and their subsequent compositional variations. In addition, multigrain XRD has been demonstrated as effective for the detection of a minor phase by indexing a few individual grains within the sample (Zhang et al. 2016); however, no additional SiO_2 or other phases were detected in this sample.

Conclusions

Multigrain XRD provides accurate unit cell determination for individual phases in a multiphase system and may serve as an in situ probe for the spatial distribution of compositional changes and/or chemical variation within a sample region of interest, complementing ex situ chemical analysis by TEM or other analysis techniques. Through careful examination of the unit cell parameters of coexisting ppv and H-phase using multigrain XRD, we characterized the compositional variations of both phases across the center area of a laser-heated sample at 119 GPa. Chemical segregation due to a large temperature gradient can be problematic in some laser heating experiments. Previous ex situ TEM analyses of recovered samples revealed strong Fe depletion and Si enrichment in the hot area, and Fe migration to the cold margin through chemical diffusion due to a relatively large temperature gradient (Sinmyo et al. 2008; Andrault and Fiquet 2001). In this study, we observed relative Fe enrichment in both phases in the heating center, relative to the margin in a well-insulated and quasi-hydrostatic sample environment at 119 GPa. The temperature gradient in the center portion (20–30 μm) of the laser-heated sample was minimized by careful experimental preparation. Therefore, the relative Fe enrichment in the center may not be driven by thermal diffusion but could be caused by the effect of temperature on the partitioning. The temperature distribution in the laser heating spot should be measured in future experiments to quantitatively understand the effect of temperature on partitioning.

Abbreviations

APS: advanced photon source; DAC: diamond anvil cell; FIB: focused ion beam; K: kelvins; opx: orthopyroxene; *P*: pressure; ppv: post-perovskite; *T*: temperature; TEM: transmission electron microscopy; XRD: X-ray diffraction.

Competing interests

The authors declare that they have no competing interests.

Authors' contributions

LZ and HKM proposed the topic and conceived and designed the study. LZ and YM carried out the experimental study. LZ analyzed the data and wrote the manuscript. YM helped in the construction of the manuscript. All authors read and approved the final manuscript.

Acknowledgements

We thank V. Prakapenka for the assistance with the experiments. This work was supported by the Foundation of President of China Academy of Engineering Physics (Grant No: 201402032) and National Natural Science Foundation of China (NSFC) (Grant No: 41574080 and U1530402). This work was also partially supported by National Science Foundation (NSF) (Grant No: EAR-1345112 and EAR-1447438). The experiments were performed at HPCAT (Sector 16) and GeoSoilEnviroCARS (Sector 13), Advanced Photon Source (APS), Argonne National Laboratory. HPCAT operations are supported by the U.S. Department of Energy—National Nuclear Security Administration (DOE-NNSA) under award DE-NA0001974 and DOE—Basic Energy Sciences (BES) under award DE-FG02-99ER45775, with partial instrumentation funding by NSF. GeoSoilEnviroCARS is supported by the National Science Foundation—Earth Sciences (EAR-1128799) and Department of Energy—Geosciences (DE-FG02-94ER14466). Use of the APS facilities was supported by the U.S. Department of Energy, Office of Science, Office of Basic Energy Sciences, under Contract No. DE-AC02-06CH11357.

Author details

[1]Center for High Pressure Science and Technology Advanced Research (HPSTAR), Shanghai 201203, China. [2]High Pressure Collaborative Access Team (HPCAT), Geophysical Laboratory, Carnegie Institution of Washington, Argonne, IL 60439, USA. [3]Geophysical Laboratory, Carnegie Institution of Washington, Washington, DC 20015, USA.

Received: 30 November 2015 Accepted: 20 April 2016
Published online: 12 May 2016

References

Andrault D, Fiquet G (2001) Synchrotron radiation and laser heating in a diamond anvil cell. Rev Sci Instrum 72(2):1283. doi:10.1063/1.1343866

Dewaele A, Loubeyre P, Mezouar M (2004) Equations of state of six metals above 94 GPa. Phys Rev B 70(9):094112. doi:10.1103/PhysRevB.70.094112

Dorfman SM, Meng Y, Prakapenka VB, Duffy TS (2013) Effects of Fe-enrichment on the equation of state and stability of (Mg, Fe)SiO3 perovskite. Earth Planet Sci Lett 361:249–257. doi:10.1016/j.epsl.2012.10.033

Fei Y, Ricolleau A, Frank M, Mibe K, Shen G, Prakapenka V (2007) Toward an internally consistent pressure scale. Proc Natl Acad Sci USA 104(22):9182–9186. doi:10.1073/pnas.0609013104

Holland TJB, Redfern SAT (1997) UNITCELL refinement from powder diffraction data: the use of regression diagnostics. Mineral Mag 61:65–77

Lundin S, Catalli K, Santillán J, Shim SH, Prakapenka VB, Kunz M, Meng Y (2008) Effect of Fe on the equation of state of mantle silicate perovskite over 1Mbar. Phys Earth Planet Inter 168(1-2):97–102. doi:10.1016/j.pepi.2008.05.002

Meng Y, Hrubiak R, Rod E, Boehler R, Shen G (2015) New developments in laser-heated diamond anvil cell with in situ synchrotron x-ray diffraction at High Pressure Collaborative Access Team. Rev Sci Instrum 86(7):072201. doi:10.1063/1.4926895

Miyahara M, Sakai T, Ohtani E, Kobayashi Y, Kamada S, Kondo T, Nagase T, Yoo JH, Nishijima M, Vashaei Z (2008) Application of FIB system to ultra-high-pressure Earth science. J Mineral Petrol Sci 103(2):88–93. doi:10.2465/jmps.070612b

Nisr C, Ribárik G, Ungár T, Vaughan GBM, Cordier P, Merkel S (2012) High resolution three-dimensional X-ray diffraction study of dislocations in grains of $MgGeO_3$ post-perovskite at 90 GPa. J Geophys Res B: Solid Earth 117(B3): n/a-n/a. doi:10.1029/2011jb008401.

Rosa AD, Hilairet N, Ghosh S, Garbarino G, Jacobs J, Perrillat J-P, Vaughan G, Merkel S (2015) In situ monitoring of phase transformation microstructures at Earth's mantle pressure and temperature using multi-grain XRD. J Appl Crystallogr 48(5):1346–1354. doi:10.1107/s1600576715012765

Schmidt S (2014) GrainSpotter: a fast and robust polycrystalline indexing algorithm. J Appl Crystallogr 47(1):276–284. doi:10.1107/s1600576713030185

Sinmyo R, Hirose K, Nishio-Hamane D, Seto Y, Fujino K, Sata N, Ohishi Y (2008) Partitioning of iron between perovskite/postperovskite and ferropericlase in the lower mantle. J Geophys Res 113(B11):B11204. doi:10.1029/2008jb005730

Sørensen HO, Schmidt S, Wright JP, Vaughan GBM, Techert S, Garman EF, Oddershede J, Davaasambuu J, Paithankar KS, Gundlach C, Poulsen HF (2012) Multigrain crystallography. Z Kristallogr 227(1):63–78. doi:10.1524/zkri.2012.1438

Tsuchiya T (2003) First-principles prediction of the P-V-T equation of state of gold and the 660-km discontinuity in Earth's mantle. J Geophys Res 108(B10):2462. doi:10.1029/2003jb002446

Tsuchiya T, Tsuchiya J, Umemoto K, Wentzcovitch RM (2004) Phase transition in $MgSiO_3$ perovskite in the earth's lower mantle. Earth Planet Sci Lett 224(3-4): 241–248. doi:10.1016/j.epsl.2004.05.017

Zhang L, Meng Y, Mao WL (2012) Effect of pressure and composition on lattice parameters and unit-cell volume of (Fe, Mg)SiO3 post-perovskite. Earth Planet Sci Lett 317–318:120–125. doi:10.1016/j.epsl.2011.11.038

Zhang L, Meng Y, Dera P, Yang W, Mao WL, Mao HK (2013) Single-crystal structure determination of (Mg, Fe)SiO3 postperovskite. Proc Natl Acad Sci USA 110(16):6292–6295. doi:10.1073/pnas.1304402110

Zhang L, Meng Y, Yang W, Wang L, Mao WL, Zeng QS, Jeong JS, Wagner AJ, Mkhoyan KA, Liu W, Xu R, Mao HK (2014) Disproportionation of (Mg, Fe)SiO3 perovskite in Earth's deep lower mantle. Science 344(6186):877–882. doi:10.1126/science.1250274

Zhang L, Popov D, Meng Y, Wang J, Ji C, Li B, Mao HK (2016) In-situ crystal structure determination of seifertite SiO_2 at 129 GPa: studying a minor phase near Earth's core-mantle boundary. Am Mineral 101:231–234. doi:10.2138/am-2015-5525